

See discussions, stats, and author profiles for this publication at: <https://www.researchgate.net/publication/235216705>

Edge curvature and convexity based ellipse detection method

Article in Pattern Recognition · September 2012

DOI: 10.1016/j.patcog.2012.02.014

CITATIONS

26

READS

226

3 authors, including:



[Dilip K. Prasad](#)

Nanyang Technological University

56 PUBLICATIONS 330 CITATIONS

SEE PROFILE

Edge curvature and convexity based ellipse detection

method

Dilip K. Prasad¹, Maylor K. H. Leung², and Siu-Yeung Cho³

¹School of Computer Engineering, Nanyang Technological University, Singapore,

²Faculty of Information and Communication Technology, Universiti Tunku Abdul Rahman (Kampar),
Malaysia,

³University of Nottingham Ningbo, China,

email: ¹dilipprasad@gmail.com

Abstract

In this paper, we propose a novel ellipse detection method for real images. The proposed method uses the information of edge curvature and their convexity in relation to other edge contours as clues for identifying edge contours that can be grouped together. A search region is computed for every edge contour that contains other edge contours eligible for grouping with the current edge contour. A two-dimensional Hough transform is performed in an intermediate step, in which we use a new ‘relationship score’ for ranking the edge contours in a group, instead of the conventional histogram count. The score is found to be more selective and thus more efficient. In addition, we use three novel saliency criteria, that are non-heuristic and consider various aspects for quantifying the goodness of the detected elliptic hypotheses and finally selecting good elliptic hypotheses. The thresholds for selection of elliptic hypotheses are determined by the detected hypotheses themselves, such that the selection is free from human intervention. The method requires a few seconds in most cases. So, it is suitable for practical applications. The performance of the proposed ellipse detection method has been tested on a dataset containing 1200 synthetic images and the Caltech 256 dataset containing real images. In both cases, the results show that the proposed ellipse detection method performs far better than existing methods and is close to the ideal results, with precision, recall, and F-measure, all very close to 1. Further, the method is robust to the increase in the complexity of the images (such as overlapping ellipses, occluded ellipses), while the performance of the contemporary methods deteriorates significantly.

Keywords: *Ellipse detection, Real images, Caltech 256 dataset, Hough transform, Overlapping ellipses, Occluded ellipses, Grouping, Saliency*

1 Introduction

Ellipse is one of the most commonly occurring geometric shapes in real images. Thus, detection of ellipses in a robust and reliable manner from real images provides us with a good image analysis tool for pattern recognition.

Besides being practically useful, ellipse detection in real images is technically a very challenging problem. This is because of many reasons that include digitization, presence of noise, lighting conditions and perspective, occlusion of objects by other objects, etc. Digitization makes the mathematically continuous elliptic shape discontinuous and distorted. Thus, the mathematically well-defined derivatives, slopes, tangents, loci, etc. do not remain valid for the digitized ellipses. The presence of noise makes the elliptic edge contours non-elliptic in certain locations or splits the continuous elliptic curve into small edge contours, such that the elliptic nature of the small edge contours is not strongly evident. Lighting condition and the perspective taken in an image may make the elliptic shapes appear as non-elliptic in an image. Further, in real images, the elliptic object may be occluded or hidden by other objects. Due to this,

complete elliptic curve may not be visible in the image and only partial curves may be available. Further, in the regions where the boundaries of two objects intersect, the edge contours may be corrupted. These problems make the detection of geometric shapes like ellipses very difficult in real images and thus technically interesting and challenging.

1.1 Literature review

Ellipse detection in real images is an open research problem since a long time. Initially, approaches like least squares fitting and Hough transform (HT) were the main approaches used by researchers. These approaches generally use the mathematical model of ellipse and the edge pixels for detecting the ellipses. Least squares based method was used for ellipse detection in [1-6]. Least squares based methods usually cast the ellipse fitting problem into a constrained matrix equation in which the solution should minimize the residue in the mathematical model. The choices of constraints and solution approaches for constrained matrix equations have an impact on the performance and selectivity of the ellipse detection methods [1, 4]. One problem with the least squares method is over-fitting of the data. Many pixels are used for ellipse detection and the elliptic hypothesis that minimizes the residue in the chosen mathematical equation and satisfies the constraint is generated. Thus, the chances of fitting an ellipse on a non-elliptic curve are high [5]. Second, though the amount of residue is used as the quality of fit and termination criterion, it may not necessarily be related directly to the quality of the detected ellipse. This is mainly because of the presence of digitization [6].

Hough transform was introduced for ellipse detection in [7] in the form of simplified Hough transform (SHT). Modifications of Hough transform, randomized Hough transform (RHT) [8, 9] and probabilistic Hough transform (PHT) [10, 11] were proposed to improve the performance of HT for non-linear problems like ellipse detection. HT based ellipse detection methods are usually more robust than least squares based ellipse detection when the edge contours are not smooth because they use pixels for detecting the ellipses instead of the edge contours (connected edge pixels) [12] while most least squares formulations for detecting ellipses use edge contours. However, HT based ellipse detection methods have two main problems. First problem is that HT is computation and memory intensive because it uses a five-dimensional parameter space. For solving the problem of five-dimensional parameters space, many methods were proposed that split the five dimensional space into two or more subspaces with lesser dimensionality and deal with each of the subspaces in separate steps [13-17]. The most popular approach in these methods was to find the centers of the ellipses using geometrical theorems and Hough transform in the first step and finding the remaining parameters of the ellipses in the second step. Second problem is that since the pixels used in HT need not belong to the same edge contour, number of samples required for detecting each ellipse is very high. Once an ellipse is detected, the pixels near the detected ellipses are not considered for the detection of the next ellipse. Due to this, HT based methods may be unable to detect all obvious ellipses (represented by edge contours) and the accuracy of such methods reduces with the increase in number of ellipses. Some methods used edge contours (instead of edge pixels) and piece-wise linear approximation of edge contours to improve the performance of HT [14, 18].

Recently, researchers have started using edge contour following methods, in which the connectivity of the edge pixels in the form of edge contours and the continuity of edge contours were used in addition to

the mathematical model of ellipse. Though the idea is old [2, 19], the effective use of the idea is fairly recent [20-25]. Evidently, use of these new tools improved the applicability of the ellipse detection methods for simple real images, typically containing one or two ellipses in foreground. These are currently the benchmark in the ellipse detection methods. However, the performance is still poor for most real images like images of the Caltech 256 dataset [26].

The edge contour following techniques group the edge contours based on continuity [20-25]. Considering one edge contour at a time, the edge contour is followed to its ends and other edge contours in the proximity of the edge contour with reasonable angular continuity with the edge contour are found. Such edge contours are then merged with the current edge contour and the newly formed edge contour after merging is followed for finding other edge contours continuous to it. Thus, effectively the parameters of continuity are used as additional constraints to the ellipse detection scheme (which may be based on least squares fitting or Hough transform or random consensus). The use of continuity as the additional constraint introduces three main problems. First, edge contour following needs recursive algorithms. Second, the edge contours that belong to a common ellipse, but are far apart cannot be grouped together based on the continuity. Third, these methods are dependent on many control parameters. For example, the continuity is typically tested using the proximity of the two edge contours and the angular deviation between them [20]. For reliable results, these parameters have to be sufficiently large so that various possible edge contours may be grouped together. However, setting large value of the parameters usually allows many more false positives and deteriorates the performance. Thus, the advantage of using continuity as a constraint is limited by the choice of several control parameters.

1.2 Introduction to the proposed method

We present a novel method that uses the information of edge curvature and convexity in relation to the other edge contours (which we shall refer to as the associated convexity for convenience) as the constraints for the ellipse detection method, instead of the conventionally used continuity constraint [20, 21, 23]. Specifically, we consider a search region for every edge contour that contains other edge contours eligible for grouping with the current edge contour. The edge contours inside the search region of an edge contour and satisfying the associated convexity are considered as the only eligible edge contours for grouping with the considered edge contour. We further increase the quality of grouping by using a two-dimensional Hough transform in an intermediate step, in which we use a new ‘relationship score’ instead of the conventional histogram count. The new relationship score is used for ranking the edge contours in a group and identifying the poorer grouping candidates in a group, which may be subsequently removed from the group if required. While the new constraints and the new relationship score improve the grouping of edge contours, which helps in improving the overall performance, additional thrust in the performance of our method comes from the novel saliency criteria, that are non-heuristic and consider various aspects for quantifying the goodness of the detected elliptic hypotheses and finally selecting good elliptic hypotheses. Thus, the novelty of the proposed method is threefold, as listed below:

1. Novel constraints based on the curvature and associated convexity of the edge contours, different from the conventionally used continuity constraint.

2. Novel relationship score that quantifies the strength of the relationship between a group and its edge contours and its use for ranking the edge contours in a group.
3. New non-heuristic saliency criteria for selecting good elliptic hypotheses.

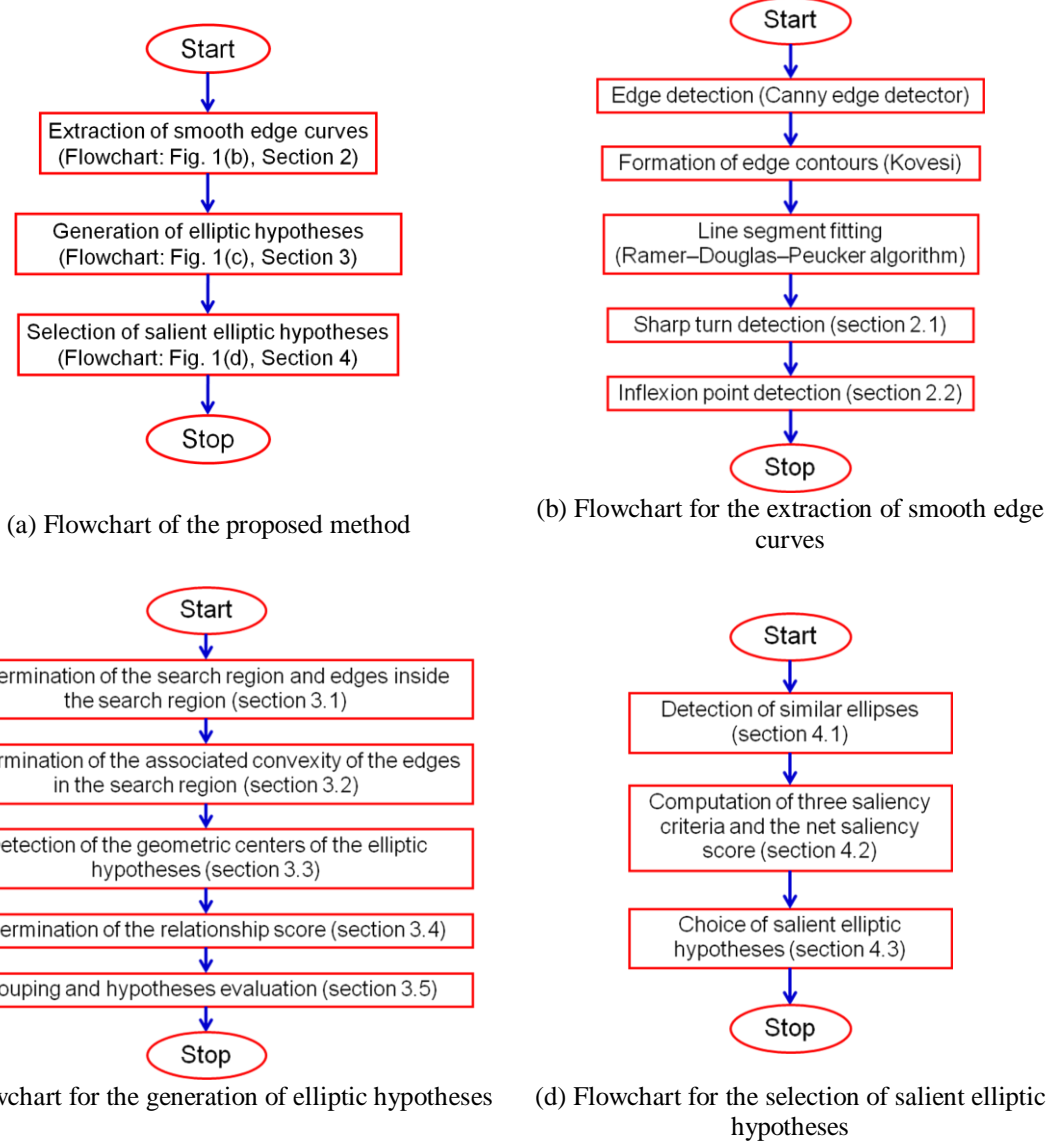


Fig. 1: Block diagram of the proposed method

The overall framework of the proposed method can be concisely presented as follows. The flowchart of the proposed method is shown in Fig. 1(a). It shows three major blocks: extraction of smooth edge curves, generation of elliptic hypotheses, and selection of salient elliptic hypotheses. In the first block (Fig. 1(b) and section 2), we extract the edge contours with smooth curvatures (smoothness as defined in section 2). This step is motivated by the fact that the curvature of the ellipse does not change sharply. The extraction of smooth edge curves is essential so that the properties of curvature and associated convexity can be used. In the second block (Fig. 1(c) and section 3), considering one edge contour at a time, we find the edge contours inside the search region of the edge contour and satisfying the associated convexity. Using the selected edge contours, we compute the centers of the elliptic hypotheses and apply HT using a method similar to [8, 17]. However, instead of using the conventional general histogram count, we use a

novel relationship score. This step of finding the centers and applying HT is not used for finding the actual parameters of the elliptic hypotheses. It is rather used for forming the groups of edge contours that potentially belong to the same ellipse, ranking the edge contours within a group, and for providing a criterion that is used for judging the elliptic hypotheses generated in the next step. After forming the groups using HT, least squares method [1] is used to evaluate the group and generate the elliptic hypotheses. The result of least squares method is evaluated using the residue in the least squares formulation as well as the center generated using the HT. If the criteria are not satisfied, poorly ranking edge contours are dropped from the group in order to improve the quality of the group. In the third block (Fig. 1(d) and section 4), we use three novel saliency criteria for selecting salient elliptic hypotheses as the output. The three criteria are combined and selection is performed such that no heuristic selection of thresholds needs to be done.

The proposed method is different from the existing methods in the following aspects:

1. The proposed method extracts the edge contours with smooth curvature in the first step, which makes the curvature analysis in the subsequent steps possible. Though approximating the edge contours using piece wise linear segments has been used before [14, 18, 20, 21, 25], it has not been used for finding the inflexion points [27, 28] and extracting the edge contours with smooth curvature.
2. The search region used in the proposed method is different from continuity constraint used in the edge contour following methods. Since the proposed search region does not use proximity or angular continuity, it is able to consider distant edge contours as the grouping candidates as well.
3. Though the study of the associated convexity has been used before [21, 29], it has been defined in complicated terms and used while selecting the edge pixels for HT [29] or for defining the angular continuity [21]. In the proposed method, associated convexity is defined using a simple mathematical equation and is used for selecting edge contours suitable for grouping.
4. The generation of the centers of elliptic hypotheses and application of HT is not used for generating the elliptic hypotheses. They are used for forming the groups of edge contours, ranking the edge contours in a group, and generating evaluation criteria for the least squares method. The use of a geometry based criterion in addition to the value of residue for the least squares fitting increases the effectiveness of least squares fitting and reduces the chances of detecting outliers.
5. We present a saliency scheme that uses three saliency scores for evaluating the goodness of the elliptic hypotheses. Most contemporary methods do use some form of saliency or distinctiveness criteria [12, 22, 23, 30-33]. The difference in the current method is that we propose three simple and effective saliency criteria, which are combined together such that the selection of the salient elliptic hypotheses is non-heuristic and no threshold or control parameters need to be specified for the selection of salient elliptic hypotheses.

1.3 Outline of the paper

The outline of the paper is as follows. The details of the three blocks in Fig. 1(b,c,d) are presented in sections 2-4 respectively. section 5 presents various sets of results to benchmark the performance of the proposed method. The article is concluded in section 6.

2 Extraction of smooth edge curves

Since it is well known that the curvature of any elliptic shape changes continuously and smoothly, we intend to obtain edge contours with smooth curvature. The term smooth curvature is defined here as follows. A portion of an edge contour which does not have a sudden change in curvature, either in terms of the amount of change or the direction of change, is called here as a smooth portion of edge contour. It should be noted that we are not performing any kind of smoothing operation. We are actually extracting curves from the existing data which are smooth as defined above. Below we explain the steps for extracting smooth edge curves. The flowchart of the process of extracting the smooth edge curves is shown in Fig. 1(b).

First, the input image is converted to gray scale. It is preferable in the case of real image to perform histogram equalization on the gray image for improving the contrast and enhancing the boundaries. Next, edge pixels are extracted from the gray image using the canny edge detector [34]. We have chosen the control parameters for Canny edge detector as follows: low hysteresis threshold $T_L = 0.1$, high hysteresis threshold $T_H = 0.2$, and standard deviation for the Gaussian filter $\sigma = 1$. This choice of control parameters works satisfactorily for most of the images. Thus, we have used these parameters for generating all our results. Then, this edge map is used to derive non-branched edge contours. For this purpose, we use Kovese's codes [35] for junction removal and extracting connected edge contours. We exclude edge contours less than 5 pixels long from further consideration since they may be the effect of noise or do not contribute in ellipse detection process due to the lack of curvature.

After extracting the edge contours, we fit line segments on each edge contour to obtain an approximate representation of the curvature of the edge contour. Here we adopt the recently proposed variation [36] of Ramer–Douglas–Peucker algorithm [37, 38] to approximate a curve into a set of line segments. This is a control parameter independent method since it does not require any control parameter. It uses an analytical upper bound for automatically determining the termination condition of the algorithm. After fitting the line segments on the edge contours, we use these line segments for extracting smooth edge curves. Beginning from one end of the edge contour, we look for points where the curvature becomes irregular and break the edge contour at those points, such that every new edge contour formed out of this process is a smooth edge contour.

Referring to the first paragraph of this section, since we define the regularity in two terms – the amount of change of curvature and the change of direction of curvature, we deal with these two cases separately and call them sharp turns and inflexion points, respectively. In the following two subsections, we present the method for detecting sharp turns and inflexion points.

2.1 Sharp turns detection

Let us consider an edge contour e , on which line segments have been fit. Let the collection of line segments that represent the edge contour e be $\{l_1, l_2, \dots, l_N\}$. Let the angles between all the pairs of consecutive line segments be denoted as $\{\theta_1, \theta_2, \dots, \theta_{N-1}\}$, where $\theta_i \in [-\pi, \pi]$ is the anticlockwise angle from l_{i+1} to l_i . An example is shown in Fig. 2(a).

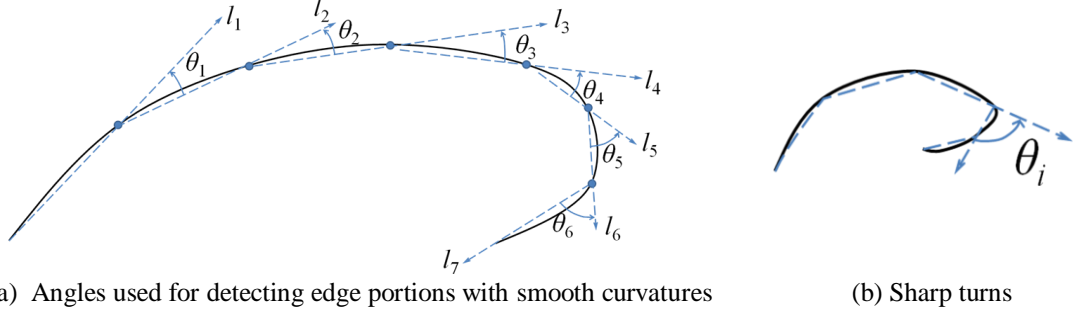


Fig. 2: Illustration of (a) the calculation of angles for detecting edge portions with smooth curvatures, and (b) sharp turns

The value of angle θ_i is an indicator of the change in the curvature of the edge contour. If θ_i is small, then it implies that the change in the curvature of the edge contour is small. On the other hand, if θ_i is large, it implies that the change in the curvature of the edge contour is large.

In the sequence of the angles, $\{\theta_1, \theta_2, \dots, \theta_{N-1}\}$, if any angle θ_i is large, i.e., equal to or greater than a chosen threshold θ_0 (say $\pi/2$, empirically determined), then the change in the curvature of the edge contour at such points P_{i+1} (the intersection point of line segments l_i and l_{i+1}) is considered to be large (or sharp), and the edge contour is split at P_{i+1} to ensure smooth curvature. An example is shown in Fig. 2(b).

2.2 Inflexion points detection

Considering the sequence of angles defined in section 2.1, $\{\theta_1, \theta_2, \dots, \theta_{N-1}\}$, the change of the sign of the angles (negative or positive) represents the change in direction of the curvature. Thus, we can create a Boolean sequence $\{b_1, b_2, \dots, b_{N-1}\}$, where b_i is given as follows:

$$b_i = \begin{cases} 1 & |\theta_i + \theta_{i+1}| < |\theta_i| + |\theta_{i+1}| \\ 0 & \text{otherwise} \end{cases} \quad (1)$$

Thus, b_i is '0' if the signs of θ_i and θ_{i+1} are the same and b_i is '1' if the signs of θ_i and θ_{i+1} are different. This Boolean sequence can be used to identify the inflexion points and decide the exact places where the edge contour should be split. It is worth noticing that there are three possibilities of the occurrence of inflexion points:

1. $b_i = 1$ AND $b_{i-1} = b_{i+1} = 0$ (in words, one '1' Boolean element between two '0' Boolean elements).

2. $b_i = 1, b_{i+1} = 1$ AND $b_{i-1} = b_{i+2} = 0$ (in words, two '1' Boolean elements between two '0' Boolean elements).
3. $b_{i-1} = 0$ AND $b_i = b_{i+1} = b_{i+2} = 1$ (in words, more than two '1' Boolean elements after one '0' Boolean element).

The possibilities, the point of splitting, and the graphical representations of the possibilities are presented in Table 1.

Table 1: Inflexion points: various possibilities

Sl. No.	Sequence	The point of split	Graphical illustration (split at the highlighted points)
1	$b_i = 1$ AND $b_{i-1} = b_{i+1} = 0$	P_{i+1}	
2	$b_i = 1, b_{i+1} = 1$ AND $b_{i-1} = b_{i+2} = 0$	P_{i+1}, P_{i+2}	
3	$b_{i-1} = 0$ AND $b_i = b_{i+1} = b_{i+2} = 1$	P_{i+1}	

Based on the absence or presence of sharp turns and inflexion points, there may be none or many points at which an edge contour needs to be split in order to obtain smooth contours. If there are N' such points on an edge contour, the edge contour can be split at these points to form $(N' + 1)$ smaller edge contours of smooth curvature.

3 Generation of elliptic hypotheses

After extracting smooth edge curves in section 2, we use the properties of the smooth curvature to form groups of edge contours that are effective for generating elliptic hypotheses. The flow chart of generation of elliptic hypotheses is shown in Fig. 1(c). The first four steps are used for finding the edge contours that are suitable for grouping. The actual grouping and elliptic hypotheses generation is done in the last step. We present the details in the following subsections.

3.1 Determination of the search region and edge contours inside the search region

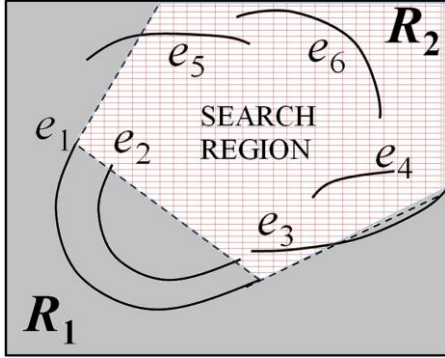
Given an edge contour of smooth curvature, a search region can be found such that the edge contours outside the search region of an edge contour can be safely excluded from grouping with the considered edge contour. Such exclusion is possible by defining a suitable search region such that the edge contours

inside the search region are the only edge contours that may be grouped with the considered edge contour for forming ellipses. Such a search region is shown in Fig. 3(a). The shaded region R_2 is the search region and the edge contours that do not lie completely inside the search region will not be grouped with e_1 .

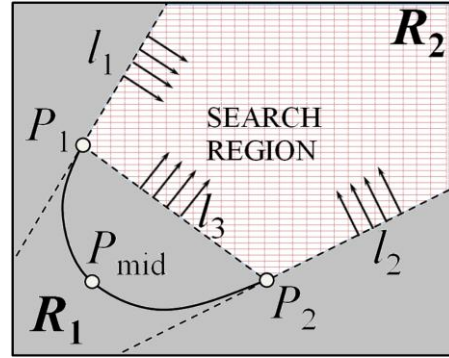
3.1.1 Finding the search region

We define the search region R as following. For a given edge contour e , let the tangents to the edge contour at its end points P_1 and P_2 be denoted by l_1 and l_2 , and the line segment connecting the end points P_1 and P_2 be denoted by l_3 . The tangents to the edge contours are computed using [39] and the value of the control parameter is chosen to be 4. The two tangents l_1 and l_2 and the line l_3 divide the image into two regions, R_1 and R_2 (notations used only for nomenclature), as shown in Fig. 3. Then the search region R is the region that does not contain P_{mid} , where P_{mid} is the middle pixel of the edge contour e . See Fig. 3(b) for illustration. Mathematically, the search region R is defined as follows:

$$R = \begin{cases} R_2 & P_{mid} \notin R_2 \\ R_1 & \text{otherwise} \end{cases} \quad (2)$$



(a) Illustration of the search region



(b) Definition of the search region

Fig. 3: Illustration and detection of the search region. The shaded region shows the search region for the edge contour e_1 . Based on the search region, it can be concluded that the edge contours e_2 , e_3 , and e_5 cannot be grouped with e_1 for generating elliptic hypotheses. The search region can be found using the lines l_1 , l_2 , and l_3 and the midpoint of the edge contour P_{mid} shown in subfigure (b).

We highlight that in Fig. 3, R_1 and R_2 are just symbolic representation of two regions. If we change the nomenclature in Fig. 3(b) then P_{mid} will not be in R_1 . Thus, according to (2), R_1 will be the search region.

3.1.2 Finding the edge contours within the search region of an edge contour

For a given edge contour e , after finding its search region R , the edge contours within the search region can be found as follows. An edge contour $e_i \in R$ if all the three criteria S1-S3 below are satisfied:

- Search region criterion 1 (S1): e_i and P_{mid} are on the same side of l_1 ,
- Search region criterion 2 (S2): e_i and P_{mid} are on the same side of l_2 , and
- Search region criterion 3 (S3): e_i and P_{mid} are on the opposite sides of l_3 .

3.2 Determination of the associated convexity of the edge contours inside the search region

The associated convexity of a pair of edge contours can be studied in order to further exclude grouping of the edge contours that are not suitable (for grouping). Fig. 4 shows five scenarios of the associated convexity between two edge contours. It is evident that the scenario presented in Fig. 4(e) is the only scenario that should be considered for optimal grouping. We present a simple method below that can identify if the two edge contours have their associated convexity as shown in Fig. 4(e).

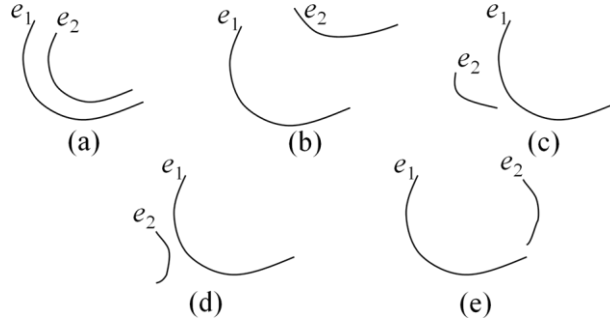


Fig. 4: Possible associated convexities between two edge contours. Only the pair in (e) should be a candidate for grouping.

Let us consider the line segments l_1 and l_2 formed by joining the end points of e_1 and e_2 , respectively, as shown in Fig. 5. Let P_1 and P_2 be the midpoints of the line segments l_1 and l_2 . Let l_3 be a line passing through P_1 and P_2 , such that it intersects the edge contours e_1 and e_2 at P'_1 and P'_2 respectively. This is illustrated in Fig. 5. The pair of edge contours e_1 and e_2 are suitable for grouping if and only if:

$$P'_1P'_2 \approx P_1P'_1 + P_1P_2 + P_2P'_2. \quad (3)$$

The approximation is attributed to the fact that P'_1 and P'_2 have to be the edge pixels nearest to the line l_3 , and may not be exactly on l_3 due to digitization of the edge pixels.

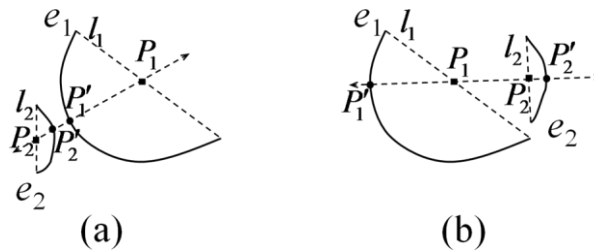


Fig. 5: Illustration of the concept of associated convexity

3.3 Detection of the geometric centers of the elliptic hypotheses

The geometrical concept used for retrieving the centers [17] is presented here. The proof of this geometrical concept is provided in [13]. Let us consider a set of three distinct pixels, $P_1(x_1, y_1)$, similarly denoted P_2 , and P_3 , on an elliptic edge contour and represent the lines tangential to the edge contour at these three points as t_1 , t_2 , and t_3 respectively. We denote the intersection point of lines t_1 and t_2 as $P_{\tan,12}$ and that of t_2 and t_3 as $P_{\tan,23}$. Further, we denote the midpoint of the line segment joining P_1 and P_2 as $P_{\text{mid},12}$ and the midpoint of the line segment joining P_2 and P_3 as $P_{\text{mid},23}$. Now, we construct a line l_{12} that passes through $P_{\text{mid},12}$ and $P_{\tan,12}$, and a line l_{23} that passes through $P_{\text{mid},23}$ and $P_{\tan,23}$. Then the centre of the ellipse is given by the intersection point of the lines l_{12} and l_{23} . The concept is illustrated in Fig. 6.

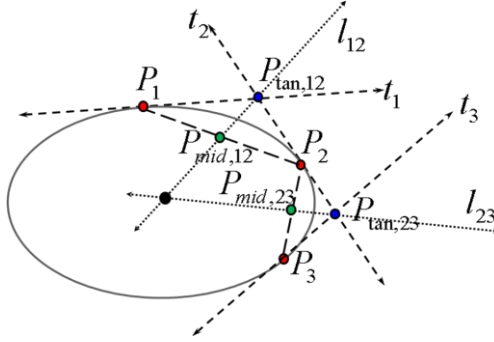


Fig. 6: Illustration of the geometric concept of finding the centre of an ellipse from three points P_1 , P_2 , and P_3 on an ellipse.

There are two geometric exceptions to the above mentioned method. First case is that t_1 and t_2 , or t_2 and t_3 are parallel to each other. Second case is that l_{12} and l_{23} are parallel to each other (i.e., the pixels in the set are collinear, though they may belong to a curved edge contour). The second case is unlikely to appear if the edge contours are of smooth curvature. In both these cases, the center of the ellipses cannot be found. In order to generate reliable estimate of the ellipse's center, many sets of points have to be generated for each edge contour.

One of the important steps in the above method is the calculation of the tangents at the chosen points. Due to the digitization of image, the tangents cannot be calculated directly. Further, changing the derivative dy/dx into differences may result into inaccurate estimation of the tangent. We have used [39] for tangent computation. Another reliable method of calculation of tangent was presented in [40].

Here, we refer to [29] for studying the effect of selection of points. Their work suggests that every pair of points in a set (of three points) should satisfy these conditions such that chances of occurrence of the above mentioned problems are reduced: (1) proper convexity, (2) proper distance between the points, and (3) reasonable angle between the tangents at these points. From this perspective, it is reasonable and

simple to split an edge contour into three sub-edge contours and choose points sequentially from each sub-edge contour. However, if the edge contour is not long enough, using this method will not ensure sufficiently high number of sets. Thus, we decide to split an edge contour into three sub-edge contours and choose points randomly from each sub-edge contour to form the desired number of sets.

The digitization in the images results into the computation of centers to be inaccurate [41]. In effect, the centers computed above cannot be used directly because the centers calculated from various sets may be close but not exactly the same. We quantize the parametric space of centers into bins. Let the input image of size $M \times N$ pixels be divided into B_m and B_n equally sized bins along the rows and columns respectively (total number of bins is $B = B_m B_n$). Thus, each bin is of size $m \times n$ pixels, where $m = M/B_m$, $n = N/B_n$.

3.4 Determination of the relationship score

Given an edge contour e , S_e sets of three pixels are generated. For each set, a centre can be computed using the geometric concept in 3.3. As discussed in section 3.3, all the sets may not generate valid centers. Let the number of sets that generated a valid center be S_e . Ideally, all S_e centers should fall in the same bin (which should coincide with the bin containing the center of the actual ellipse). In practice, all the computed centers will not fall in the same bin.

We propose to assign a score to each bin-edge contour pair, which we shall refer to as the relationship score. The relationship score is an indicator of the trust that can be put upon their relationship. All the edge contours in a single bin are considered as a group (potentially belonging to a common ellipse). However, they are ranked on the basis of their score within a group.

A simple relationship score can be:

$$\tilde{r}_e^b = S_e^b \quad (4)$$

where $S_e^b \leq S_e$ is the number of sets of the edge contour e that voted for the bin b . The count of the votes for bin b , commonly referred to as the general histogram count, is therefore $\left(\sum_{\forall e} \tilde{r}_e^b \right)$. Below, we present the novel relationship score r_e^b (which can be considered as an enhancement of \tilde{r}_e^b) as follows:

$$r_e^b = S_e^b r_1 r_2 \quad (5)$$

where, r_1 is a function of S_e^b/S_e and r_2 is a function of S_e/S . For avoiding confusion, we reiterate that \tilde{r}_e^b of (4) is used for general histogram count, and r_e^b of (5) is the proposed relationship score.

The ratio $S_e^b/S_e \in [0,1]$ is an indicator of the relative weight of the bin b as compared to other bins that were computed for the same edge contour. If S_e^b/S_e is high, the bin is better ranked than the rest of the bins, indicating that the relation between the edge contour and the bin b is stronger, and thus should be given more priority. On the other hand if S_e^b/S_e is less, the bin might have been computed by a chance

combination of the randomly selected pixels, and should not be given significant importance. A non-linear r_1 as shown in Fig. 7(a) is preferred to dampen r_e^b for low S_e^b/S_e . We compute r_1 as follows:

$$r_1 = \left(\frac{S_e^b}{S_e} \right) \exp \left(\frac{S_e^b}{S_e} - 1 \right), \quad (6)$$

where $\exp(\bullet)$ denotes the exponential function. Though other functions might be chosen to achieve similar effect, this is not the scope of the current work to compare with other types of functions. Here, it suffices to say that the above function emulates well the desired effect.

As discussed before, out of the total S sets generated for an edge contour, all may not result into valid bins. If there are only a few valid sets S_e in comparison to S , it may mean that the edge contour is a poor elliptic candidate (and thus an outlier). On the other hand, if the ratio $S_e/S \in [0,1]$ is high, then it is indicative of the edge contour being a good elliptic arc. Similar to r_1 , we set r_2 as follows:

$$r_2 = \left(\frac{S_e}{S} \right) \exp \left(2 \left(\frac{S_e}{S} - 1 \right) \right), \quad (7)$$

where r_2 has stronger dampening effect than r_1 . It should also be noted that while r_1 is indicative of relative importance of a bin (among various bins computed for an edge contour), r_2 is indicative of the relative trust of an edge contour (in comparison to other edge contours).

In order to illustrate the effect of using the relationship score as compared to the general histogram typically used in Hough transform, we consider a simple image of size 300×300 pixels shown in Fig. 7(b). We use $m = n = 10$ pixels for forming the bins. We compute the total histogram count per bin $\left(\sum_{\forall e} \tilde{r}_e^b \right)$ and total relationship score per bin $\left(\sum_{\forall e} r_e^b \right)$ and plot them in Fig. 7(c,d) respectively. We also plot the bins which received non-zero (white) histogram count and relationship score in Fig. 7(e,g) respectively. Fig. 7(f,h) show bins with values $> 0.01 \max \left(\sum_{\forall e} \tilde{r}_e^b \right)$ and $> 0.01 \max \left(\sum_{\forall e} r_e^b \right)$ respectively. In Fig. 7(e-h), the actual centers of the ellipses are shown using asterisks (*).

It is seen that Fig. 7(e-g) are exactly the same. The similarity of Fig. 7(e,g) can be understood from the fact that if there is a non-zero vote in a bin, both $\left(\sum_{\forall e} \tilde{r}_e^b \right)$ and $\left(\sum_{\forall e} r_e^b \right)$ are non-zero. On the other hand, if a bin has zero votes, both $\left(\sum_{\forall e} \tilde{r}_e^b \right)$ and $\left(\sum_{\forall e} r_e^b \right)$ are zero. Fig. 7(f) is same as Fig. 7(e) because no bins have been filtered away when 1% filtering is used on $\left(\sum_{\forall e} \tilde{r}_e^b \right)$. On the other hand, with 1% filtering on $\left(\sum_{\forall e} r_e^b \right)$, many bins are filtered away, as shown in Fig. 7(h). It is clearly visible that the proposed

relationship score is more selective than the general histogram count even when only 1% filtering is used

for $\left(\sum_{\forall e} \tilde{r}_e^b\right)$ and $\left(\sum_{\forall e} r_e^b\right)$ to eliminate irrelevant center hypotheses.

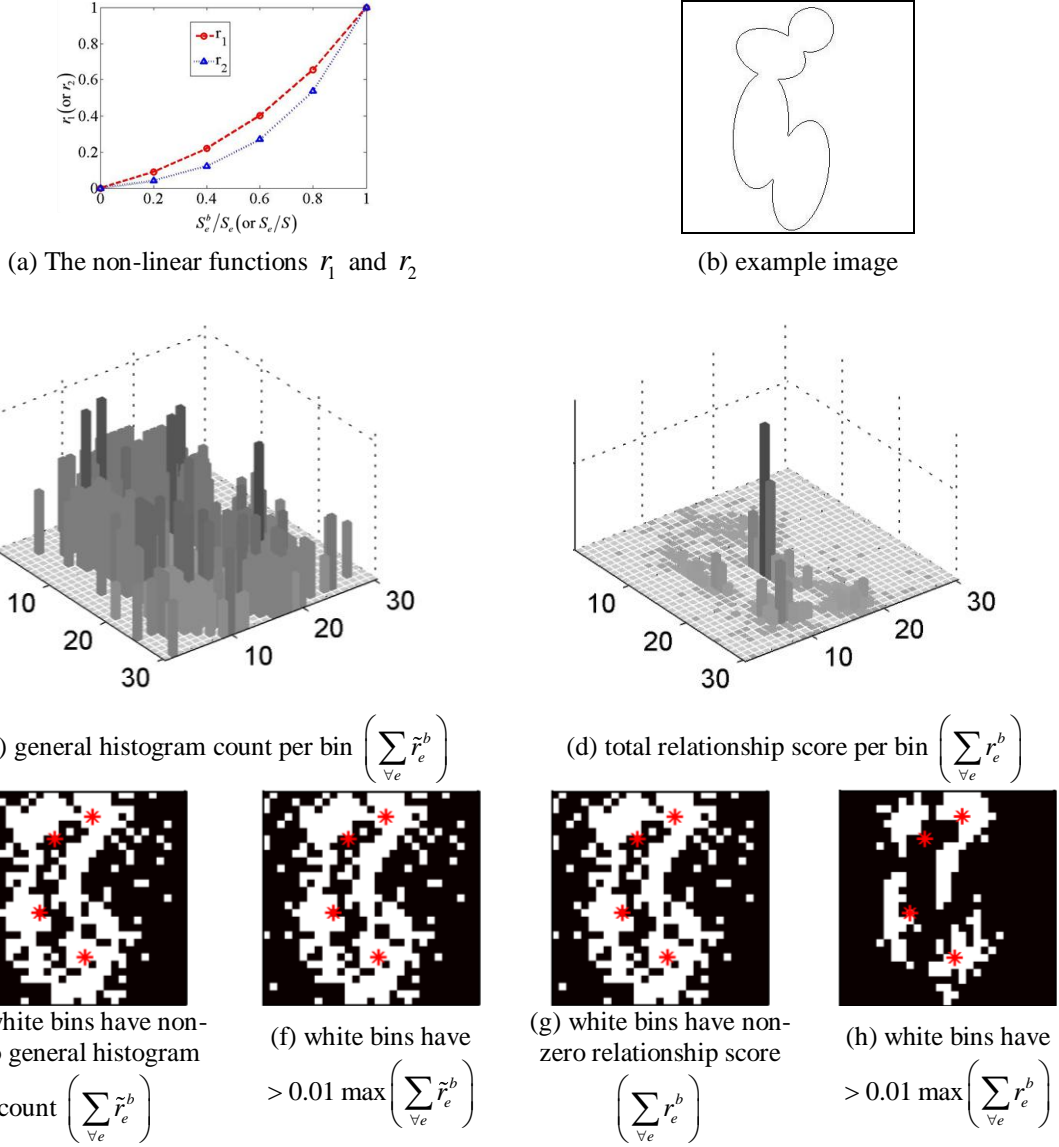


Fig. 7: The proposed relationship score and its effect (asterisks in (e-h) denote the actual centers of the ellipses in (b)).

Thus, the specific advantages of the proposed relationship score over the conventional histogram count used in Hough transform are listed as follows:

1. The relationship score is more selective than the conventional histogram count. Since we use this step as initial guess for grouping, the selective nature of relationship score is expected to generate fewer but better groups. This increases the reliability of this step as initial guess and reduces the computational complexity of the complete scheme.

2. While the general histogram count (or \tilde{r}_e^b) is insensitive to the information in S_e^b/S_e and S_e/S regarding the edge contour, the relationship score r_e^b uses this information to generate a fairer score for ranking the edge contours within a group.

3.5 Grouping and hypotheses evaluation

The following method is used for grouping the edge contours that possibly belong to a common ellipse and finding the remaining parameters of the elliptic hypothesis. Here, grouping does not mean physical merging/connecting of the edge contours. In the current context, grouping means collecting the edge contours that may possibly belong to same ellipse as one set.

After assigning the relationship score r_e^b , all the edge contours having a common bin b may initially be considered as a group. The various edge contours in a group are ranked based on their bin-edge contour relationship scores r_e^b . The edge pixels of the edge contours in a group are appended in the descending order of their relationship scores r_e^b and least squares fitting technique [1]¹ is used on the group to find all the parameters of the ellipse. Now, we evaluate the quality of this group based on two criteria listed below:

- Criterion 1 (C1): Error of least squares fitting $\leq \varepsilon_{ls}$, a chosen threshold error value.
- Criterion 2 (C2): The centre bin b of the group is inside the detected elliptic hypothesis.²

If both C1 and C2 are satisfied, then the parameters of the ellipses computed using the least squares fitting are given as output. If anyone of the two criteria is not fulfilled, the weakest edge contour (with the lowest relationship score r_e^b) is removed from the group and the above process is repeated till either the above criteria are satisfied or the group becomes empty.

4 Selection of salient elliptic hypotheses

The above elliptic hypotheses generation scheme may generate multiple elliptic hypotheses corresponding to an actual ellipse because various groups may correspond to a common ellipse. We perform the elliptic hypotheses selection in two stages. In the first stage, we find out the hypotheses that are similar to each other and keep only one representative elliptic hypothesis among them (section 4.1). This increases the chances of one elliptic object being represented by a single elliptic hypothesis. In the second stage, the elliptic hypotheses that remain after the clustering are evaluated for their saliency. We present three kinds of saliency criteria and methods to combine them in section 4.2. Using an example, we study the effectiveness of the saliency scores and their combinations in section 4.2.6. Based on the study, the proposed selection scheme is provided in section 4.3.

¹ Two changes have been done in implementing [1]: 1) The data is zero mean shifted before applying [1] for better numerical stability. 2) If the method in [1] generates illogical values of the parameters of ellipse (for example negative or imaginary value of semi-major and semi-minor axis, or imaginary values of center coordinates), then the least square error is set to a value larger than ε_{ls} .

² If the quadratic equation of the ellipse is given by $f(x, y) = 0$, then a bin b is inside the ellipse if the center of the bin (x_b, y_b) is such that $f(x_b, y_b) < 0$.

4.1 Detection of similar ellipses

Let the quadratic equation describing an ellipse be:

$$f(x, y) = 0 \quad (8)$$

A pixel $P(x', y')$ in the image belongs to the elliptic region (inside or on the boundary of the ellipse) if $f(x', y') \leq 0$. Using this concept, the image pixels outside the ellipse can be labeled Boolean '0', while the rest can be labeled Boolean '1'. Let the two dimensional matrix that stores these Boolean variables for various pixels be denoted as I . Suppose we intend to find if two ellipses E_1 and E_2 are similar. We obtain the Boolean matrices I_1 and I_2 , using the quadratic functions $f_1(x, y)$ and $f_2(x, y)$ respectively. Then we define the following similarity measure:

$$D = 1 - \frac{\text{count}(XOR(I_1, I_2))}{\text{count}(OR(I_1, I_2))} \quad (9)$$

where $\text{count}(A)$ gives the number of Boolean '1' elements in the matrix A . Here, $XOR(I_1, I_2)$ gives Boolean values '1' at the pixels which belong to only one of the ellipses (and not both), i.e. the non-overlapping region of the ellipses. $OR(I_1, I_2)$ gives the total region jointly overlapped by the two regions. Thus D gives the ratio of overlap of the two ellipses. We note that the above overlap ratio is an adaptation of the Jaccard index used in set theory [42]. The concept is illustrated graphically in Fig. 8.

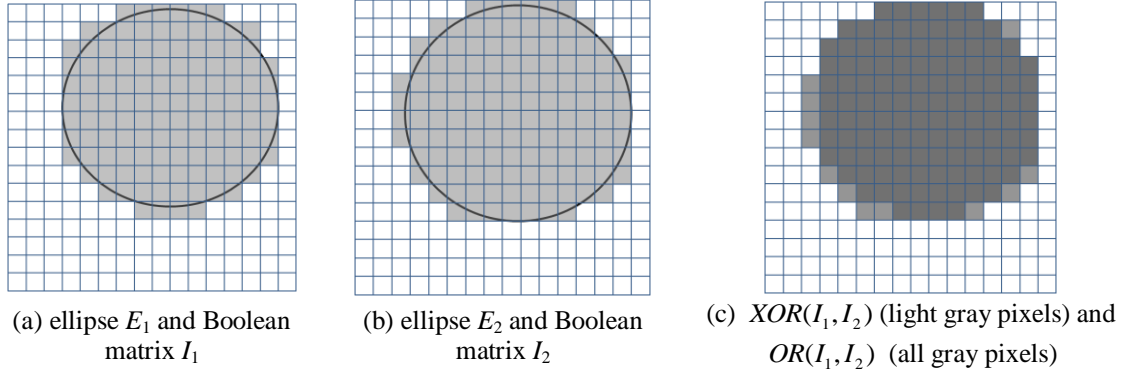


Fig. 8: The illustration of the concept of overlap measure.

For a given ellipse, all the ellipses that have overlap ratio $D > D_0$; $D_0 = 0.9$ are clustered together. Among the ellipses in a cluster, the choice of representative candidate should depend upon the reliability of the ellipses in the cluster. One way of determining the reliability is to choose the ellipse that was formed by maximum amount of data. Thus, we have used the angular circumference ratio (introduced in section 4.2.1).

4.2 Computation of three saliency criteria

We use the following three criteria (detailed in the following subsections) for computing the saliency of the elliptic hypotheses:

1. Angular circumference ratio

2. Alignment ratio
3. Angular continuity ratio

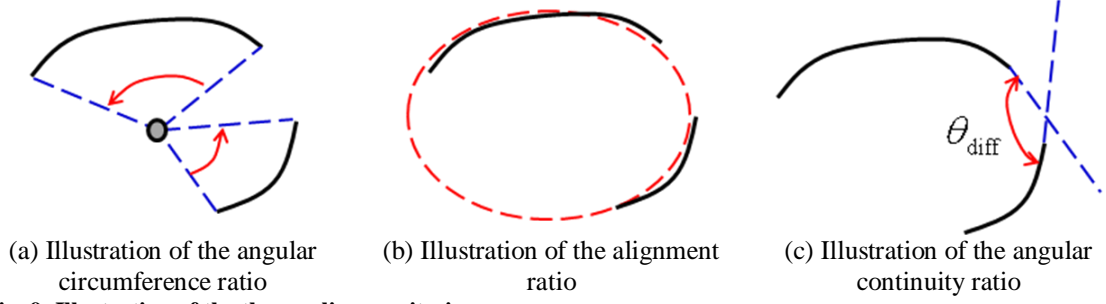


Fig. 9: Illustration of the three saliency criteria

4.2.1 Angular circumference ratio

Instead of using the pixel count feature [30], we use the angle subtended by an edge contour on the center of the ellipse as the measurement of circumference (as illustrated in Fig. 9(a)). Such scheme is less sensitive to the quantization problem in the pixel count feature. Suppose an ellipse E was fitted to a group G , then we define a function $c(E, G)$ as below:

$$c(E, G) = \frac{\sum_{e \in G} \alpha(E, e)}{2\pi} \quad (10)$$

where $\alpha(E, e)$ is the angle subtended by the ends of the edge contour e at the centre of the ellipse E . A higher value of $c(E, G)$ implies a larger support of E on G .

4.2.2 Alignment ratio

This saliency criterion considers the distribution of the pixels around the elliptic hypothesis as shown in Fig. 9(b). This idea was first proposed by [32], though in the context of straight lines primarily. In the context of elliptic hypotheses, we present the following method.

We consider the pixels $\{P\}$ in the edge contour that generated an elliptic hypothesis, and compute their Euclidean distance, d , from the elliptic hypothesis. The lesser the Euclidean distance, the more reliable is an edge pixel for generating the elliptic hypothesis. After applying a threshold ($d_0 = 2$) on the Euclidean distance, we count the number of pixels that are reliable for the current hypothesis and normalize it with respect to the total number of pixels, N_G , in the edge contours that generated the hypothesis as shown below:

$$s(E, P) = \begin{cases} 1 & \text{if } d < d_0 \\ 0 & \text{otherwise} \end{cases} \quad (11)$$

$$a(E, G) = \frac{\sum_{i=1}^{N_G} s(E, P_i)}{N_G} \quad (12)$$

The higher the value of $a(E, G)$, the better is the fit between ellipse E and group G .

4.2.3 Angular continuity ratio

Another criterion for choosing salient hypotheses is based on the angular continuity of the edge contours that generated a hypothesis. Let us consider two edge contours as shown in Fig. 9(c). The angle between the two intersecting tangents made at the two nearest end points of e_1 and e_2 , θ_{diff} , is the angle that determines the continuity between the two edge contours. It can have a maximum value π . Thus, the ratio of the angle, θ_{diff} , and π is an indicator of the continuity between the two edge contours. Similar idea was proposed in [23].

The angular continuity ratio is defined as:

$$\phi(E, G) = \begin{cases} 1 & \text{if } N = 1 \\ \frac{1}{N-1} \sum_{i=1}^{N-1} \frac{\theta_{\text{diff}}(e_i, e_{i+1})}{\pi} & \text{if } N > 1 \end{cases} \quad (13)$$

where N is the number of edge contours in the group G . It is worth noting that if an elliptic object has large $\phi(E, G)$, the reliability of such elliptic hypotheses is better than an elliptic object that appears in the form of far apart contours.

4.2.4 Determination of the net saliency score

All the three criteria discussed in section 4.2 are representative of the quality of an elliptic hypothesis in the context of the image. While all of them have their respective strengths, all of them have their own deficiencies. Combining them to form a single saliency measure works as supplementing their individual capabilities. In what follows, we present and discuss various methods of combining the three saliency criteria.

4.2.4.1 Multiplicative combination

The first way of combining them is to multiply the three criteria as follows. The net saliency of an ellipse E detected using a group G is the product of $a(E, G)$, $c(E, G)$, and $\phi(E, G)$:

$$\sigma_{\text{mul}}(E, G) = a(E, G) c(E, G) \phi(E, G). \quad (14)$$

The net saliency as defined above takes into account each of the three criteria. Due to its multiplicative nature, if any of the criteria is very poor, the net saliency of the hypothesis becomes very low, even though it might be salient in terms of the other two criteria. In effect, it works similar to Boolean AND

function. Thus, on one hand it rewards the hypotheses that are salient in terms of all three criteria, on the other hand it is very strict on the rest.

4.2.4.2 Additive combination

The problem with multiplicative combination motivates us to consider the additive combination of the three criteria. Given the fact that the range of all the three criteria is $[0,1]$, the value 1 being the most desirable, we may consider the net saliency as the average of the three criteria as follows:

$$\sigma_{\text{add}}(E, G) = \frac{a(E, G) + c(E, G) + \phi(E, G)}{3} . \quad (15)$$

While the multiplicative combination is too sensitive to the poor performance of any criterion, the additive combination is less sensitive to the poor performance of a single criterion. This means that though one of the criteria may have low value, if the other two criteria have sufficiently high values, the net saliency in additive combination will still be sufficient to have the hypothesis selected.

4.2.5 Choosing a threshold

Whatever be the saliency measure, higher value of saliency indicates that the detected ellipse is better than the ellipses with lower saliency. Based on this value, the best ellipses can be determined in various ways. The most prevalent and straight forward manner is to choose all the ellipses with saliency higher than a threshold. The performance of the ellipse detection method greatly depends upon the choice of the threshold. However, there is typically no hard and fast rule that ensures the suitability of a chosen threshold in most scenarios. The value that seemingly works very well for one image(s) may completely fail in another image(s). On the other hand, we propose to use the statistical mean of the net saliency for all the elliptic hypotheses as the threshold. Once the saliency measure is computed for each elliptic hypothesis, the average of all the saliency measures can be computed and used as the threshold. The scheme proposed by us is presented in more detail in section 4.3. Our observation is that it works well for most images.

4.2.6 Example

In order to further elucidate the discussion above, we present an example image and study the various saliency criteria, the multiplicative and additive saliency scores, and the effect of using a threshold for selecting the hypotheses. The examples is presented in Fig. 10. In the example, the smooth edge contours are extracted according to the procedure in section 2 (see Fig. 10(c)). The proposed method (till section 4.1) is used for generating elliptic hypotheses. After generating the elliptic hypotheses and removing similar ellipses, we compute the three saliency criteria discussed in section 4.2 for each elliptic hypotheses. We also compute the multiplicative net saliency score (14) and additive net saliency score (15) for each elliptic hypotheses. For reference, we show the elliptic hypotheses chosen by the proposed elliptic hypotheses selection scheme (section 4.3) in Fig. 10(d) .


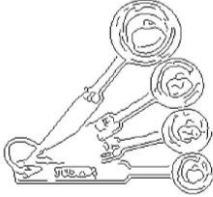
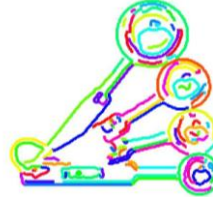
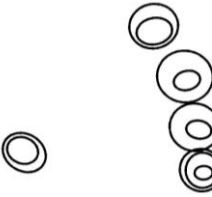





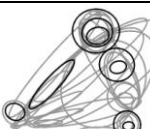
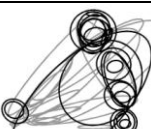

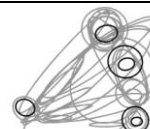
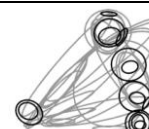
				
(a) Original image	(b) Canny edge map	(c) Smooth edge curves (section 2)	(d) Ellipse detection using the proposed saliency score (16)	
				
(e) angular circumference ratio of various elliptic hypotheses (10). The darker ellipses indicate high value of $c(E, G)$	(f) alignment ratio of various elliptic hypotheses (12). The darker ellipses indicate high value of $a(E, G)$	(g) angular continuity ratio of various elliptic hypotheses (13). The darker ellipses indicate high value of $\phi(E, G)$	(h) multiplicative combination of the three saliency criteria (14). The darker ellipses indicate high value of $\sigma_{mul}(E, G)$	(i) additive combination of the three saliency criteria (15). The darker ellipses indicate high value of $\sigma_{add}(E, G)$
				
(j) Ellipses with $c(E, G) \geq$ $0.8 \max(c(E, G) \forall E)$ are shown in dark color. Others are in light color	(k) Ellipses with $a(E, G) \geq$ $0.8 \max(a(E, G) \forall E)$ are shown in dark color. Others are in light color	(l) Ellipses with $\phi(E, G) \geq$ $0.8 \max(\phi(E, G) \forall E)$ are shown in dark color. Others are in light color	(m) Ellipses with $\sigma_{mul}(E, G) \geq 0.8$ $\max(\sigma_{mul}(E, G) \forall E)$ are shown in dark color. Others are in light color	(n) Ellipses with $\sigma_{add}(E, G) \geq 0.8$ $\max(\sigma_{add}(E, G) \forall E)$ are shown in dark color. Others are in light color

Fig. 10: Example: Illustration of the saliency criteria, the multiplicative combination, the additive combination, and the proposed selection of salient elliptic hypotheses (16).

In subfigures (e)-(g) of Fig. 10, we plot the results of the three saliency scores (section 4.2.1 - 4.2.3). In subfigures (h)-(i) of Fig. 10, we plot the result of the multiplicative and additive net saliency scores (section 4.2.4). In these subfigure, the darkness of an elliptic hypothesis is proportional to the value of the score. This means that darker ellipses have higher value of the presented score as compared to the lighter ellipses.

Now, we apply a threshold of 0.8 on each of the saliency scores. This means that for a particular saliency score, we choose the ellipses that have a score of greater than or equal to 0.8 times the maximum score (for all elliptic hypotheses). In subfigures (j)-(l) of Fig. 10, we plot the elliptic hypotheses chosen by applying the threshold 0.8 on the three saliency scores (section 4.2.1 - 4.2.3). In subfigures (m)-(n) of Fig. 10, we plot the elliptic hypotheses chosen by applying the threshold 0.8 on the multiplicative and additive net saliency scores (section 4.2.4). The chosen elliptic hypotheses are shown in the dark, while the remaining elliptic hypotheses are shown in light color.

The first observation is that none of the saliency criteria performs well in choosing the elliptic hypotheses. The circumference ratio (Fig. 10(e,j)) performs better than the remaining saliency criteria (Fig. 10(f,g,k,l)). While alignment ratio (Fig. 10(f,k)) is able to select the true positive elliptic hypotheses,

it is not able to reject the false positive elliptic hypotheses effectively. The angular continuity ratio performs better than the alignment ratio. Thus, use of a single saliency criterion is not reliable for diverse images.

Second observation is that the multiplicative net saliency score (Fig. 10(h,m)) is more selective than the additive net saliency score (Fig. 10(i,n)). Only the elliptic hypotheses that have high scores in all the three saliency criteria stand a chance to get selected using the multiplicative net saliency score (Fig. 10(h,m)). As already discussed before, the saliency criteria may behave differently in different images. Thus, only very good elliptic hypotheses are selected by the multiplicative combination. As a consequence, multiplicative net saliency score will give good precision but significantly poor recall.

4.3 The proposed scheme for hypotheses selection

As shown using the example in section 4.2.6, neither the multiplicative combination, nor the additive combination is suitable for elliptic hypotheses selection. Further, the suitable threshold for selecting the elliptic hypotheses varies from image to image. In order to make the selection of the elliptic hypotheses non-heuristic, the decision of selecting the elliptic hypothesis E is made using the expression below:

$$\text{AND} \left(\begin{array}{l} a(E, G) \geq \text{avg} \{a(E, G)\}, \\ c(E, G) \geq \text{avg} \{c(E, G)\}, \\ \phi(E, G) \geq \text{avg} \{\phi(E, G)\}, \\ \sigma_{add}(E, G) \geq \text{avg} \{\sigma_{add}(E, G)\} \end{array} \right) \quad (16)$$

Here, $\text{avg} \{a(E, G)\}$ is the average value of the alignment ratios calculated for all the elliptic hypotheses remaining after the similar ellipses identification. The same applies for the other expressions in (16). The use of the average values of the saliency scores as the threshold for selection makes the selection procedure non-heuristic and free of human intervention. This is unlike other methods where thresholds are chosen based on heuristics and their efficacy depends largely on the considered application and dataset. Our selection method chooses the appropriate threshold values in (16) for each image independently and is therefore not dependent on the type of dataset.

Further, the use of AND operation ensures that the elliptic hypotheses that are good in every respect are selected finally. This selection method assures that the selected hypotheses perform better than the average elliptic hypotheses (for a particular image) in every criterion and have overall good saliency. Due to the non-heuristic thresholds and the AND operation, our ellipse detection method is able to generate good results for a large variety of images as demonstrated by the numerical results in the following section.

5 Numerical Results

We present various numerical results to test the proposed ellipse detection method. We consider two types of dataset: dataset of synthetic images and dataset of real images. These datasets are discussed in sections 5.1 and 5.2 respectively. The comparison metrics used to test the performance of the ellipse

detection methods are presented in section 5.3. The performance of the proposed method is compared against five other ellipse detection methods in section 5.4.

5.1 Synthetic dataset: overlapping and occluded ellipses

We test the proposed method under various scenarios such as occluded ellipses and overlapping ellipses using synthetic images. To generate the synthetic images, we consider an image size of 300×300 and generate $\alpha \in \{4, 8, 12, 16, 20, 24\}$ ellipses randomly within the region of image. The parameters of the ellipses are generated randomly: center points of the ellipses are arbitrarily located within the image, lengths of semi-major and semi-minor axes are assigned values randomly from the range $[10, 300/\sqrt{2}]$, and the orientations of the ellipses are also chosen randomly. The only constraint applied is that each ellipse must be completely contained in the image and overlap with at least one ellipse.

For each value of α , we generate 100 images containing occluded ellipses and 100 other images containing overlapping ellipses. In the occluded ellipses, the edge contours of the overlapped regions are not available, while in the overlapping images all the edge contours of the ellipses are available. Thus, in total there are 600 images with occluded ellipses and 600 images with overlapping ellipses. In Fig. 15 and Fig. 16, examples of synthetic images and the detected elliptic hypotheses are presented.

5.2 Real image dataset

We have used the Caltech-256 database [26] as the dataset for real images. These images present greater challenges than those tested above due to corruption of the contours of elliptical shaped objects by complex and varied backgrounds, illumination variations, partial occlusions, image noise, shadows and spectral reflections. In the Caltech 256 dataset, 400 real images were randomly chosen from 48 categories. Only one condition was used for selection. At least 5 (among 20 volunteers) should identify a minimum of one recurring ellipse as the ground truth. The ground truth has been generated for each image by 20 volunteers. For each image, the elliptic clusters³ voted by more than 10 volunteers are considered as the global ground truth. Among the 400 real images used for generating the results, the minimum number of ellipses in an image was 1 and the maximum number of ellipses was 60.

5.3 Comparison metrics and the experimental setup

We present results for the proposed algorithm on a set of challenging synthetic and real images. The following metrics are used for evaluating the performance of the proposed ellipse detection method:

$$\text{Precision} = \frac{\text{number of true positive elliptic hypotheses}}{\text{total number of elliptic hypotheses}} \quad (17)$$

$$\text{Recall} = \frac{\text{number of true positive elliptic hypotheses}}{\text{number of actual ellipses}} \quad (18)$$

³ An elliptic cluster is a cluster in which all the ellipses have an overlap of more than 0.9 with each other. The hypothetical ellipse that is computed using the average parameters of the ellipses within a cluster is used to represent the cluster.

$$\text{F-measure} = \frac{2 \times \text{Precision} \times \text{Recall}}{\text{Precision} + \text{Recall}} \quad (19)$$

where the true positive elliptic hypotheses are the hypotheses that have high overlap with the ellipses in the ground truth. For synthetic dataset, an overlap ratio of 0.95 is used for determining true positive hypotheses (Fig. 15 and Fig. 16). Considering the more complex nature of the real images as compared to synthetic images, an overlap ratio of 0.8 is used for determining the true positive hypotheses in the real images dataset.

For the synthetic dataset (occluded ellipses), the performance metrics are computed for each of the 100 images corresponding to a value of α , and the mean for 100 images is used as the performance metric for that value of α . Similar procedure is used for the synthetic images containing the occluded ellipses. For real images, the average of the performance metrics for the 400 images are used as the overall representative performance metrics of the real dataset.

We use square bins of size 25×25 pixels based on the guidelines in [41, 43], and set the threshold for C1 as $\varepsilon_{ls} = 0.01$. The number of sets used for finding the centers of elliptic hypotheses (section 3.3) using an edge contour is $S = 200$.

5.4 Performance comparison with other methods

The performance of the proposed method is compared against one standard ellipse detection method and four recently proposed ellipse detection methods. The standard method considered is the randomized Hough transform (RHT) [8]. The recently proposed methods considered here are the methods proposed by Mai [20], Kim [21], Bai [28], and Liu [44]. For Bai [28] and Liu [44], the values of control parameters used in their original works did not provide good results. Thus, the control parameters were varied and the best combination of control parameters were obtained to get the best results for synthetic images (Bai [28]: $\text{disTh} = 0.03$, $\text{dMinTh} = 10$, $\text{dTh} = 3.0$ and Liu [44]: $\eta = 1/N$, $e_{th} = 0.05$, $\alpha = 0.1$, other control parameters retain the default value of the respective algorithm). We highlight that these methods are very sensitive to the choice of control parameters. For instance, using $\text{disTh} = 0.009$ as mentioned in Table 2 of Bai [28], results in less than 5% precision for synthetic datasets and almost no detections for real dataset. Similarly, using $\alpha = 0.5$, as suggested in [44] results in almost zero precision for synthetic and real datasets.

The results for synthetic dataset are presented in Fig. 11 (occluded ellipses) and Fig. 12 (overlapping ellipses). It is clearly evident that the proposed method outperforms the existing methods in terms of precision, recall, as well as F-measure. Further, it is close to the best values of precision, recall, and F-measure (the best value is 1 for all these measures). Lastly, even with substantial increase in the number of ellipses in an image, the performance does not deteriorate significantly. The proposed method took an average time of 5.63 seconds for the synthetic dataset.

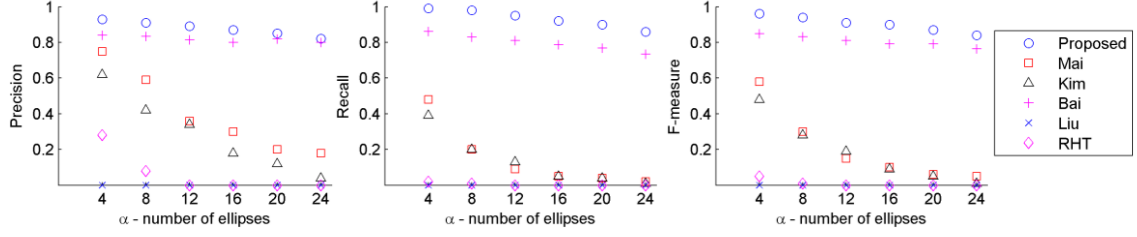


Fig. 11: Comparison of the proposed method with other methods for images with occluded ellipses (synthetic dataset).

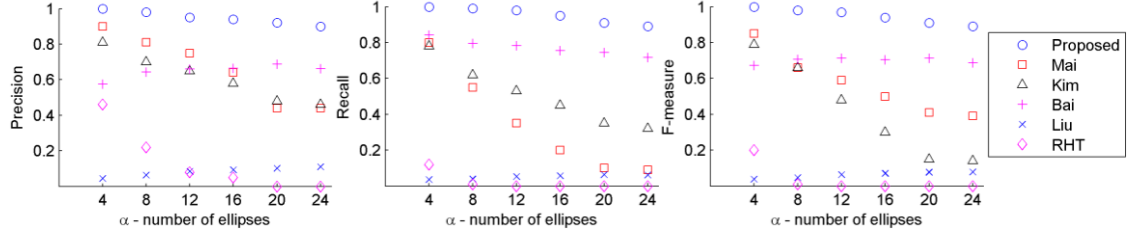


Fig. 12: Comparison of the proposed method with other methods for images with overlapping ellipses (synthetic dataset).

We note that Liu [44] has zero detections for the case of occluded ellipses. This is because Liu [44] does not deal with the inflexion points, as also highlighted in [44]. We also note that Bai [28] gives the closest and most consistent performance with respect to the proposed method for the case of occluded ellipses. This is consistent with the nature of dataset considered in Bai [28]. However, it performs poorer for the case of overlapping ellipses as compared to the occluded ellipses. The performance is further deteriorated for real images, as seen in Table 2. Mai [20] and Kim [21] show deteriorating performance as the number of ellipses increases.

As mentioned before, for synthetic images, we used an overlap ratio of 0.95 between the elliptic hypotheses and the ground truth (true parameters of the ellipses) for determining the true positive hypotheses. In order to show that the poor performance of the other methods is not due to the high overlap ratio, we further test the performance of our method and the other methods using different values of the overlap ratio used for determining the true positive hypotheses. For this purpose, we use images with $\alpha = 12$. The comparison results of the proposed method and the other methods are shown in Fig. 13 and Fig. 14. It is evident that the performance of the proposed method does not depend significantly on the overlap ratio used for finding the true positive elliptic hypotheses.

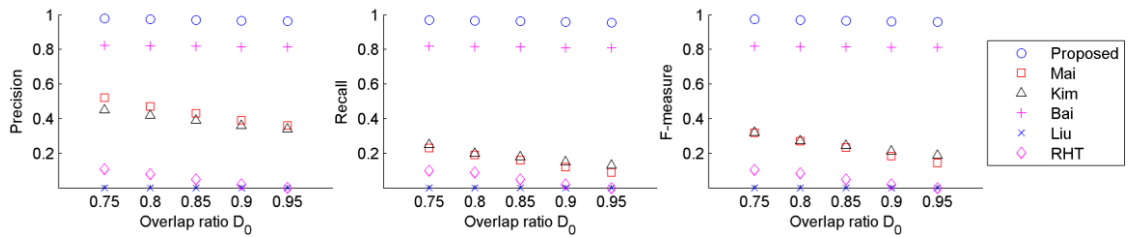


Fig. 13: Comparison of performance of the proposed method with other methods for synthetic images with $\alpha = 12$ occluded ellipses considering various values of the overlap ratio for finding the true positive elliptic hypotheses.

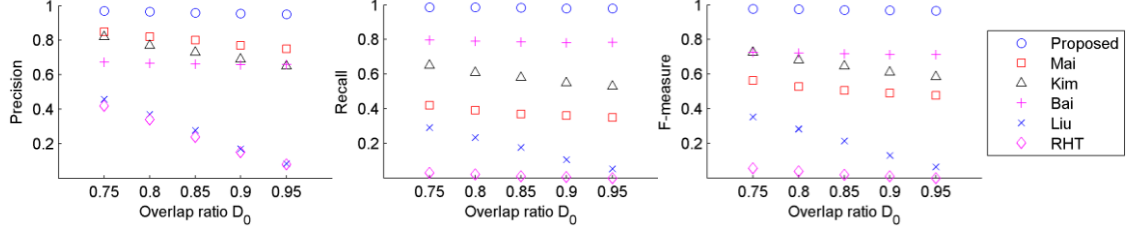


Fig. 14: Comparison of performance of the proposed method with other methods for synthetic images with $\alpha = 12$ overlapping ellipses considering various values of the overlap ratio for finding the true positive elliptic hypotheses.

Now, we compare the performance of various methods and the proposed method for the real image dataset. The average values of the performance metrics for the 400 real images from 48 categories of the Caltech 256 [26] are shown in Table 2. The total time taken by each method for the complete dataset is also shown. In terms of the performance, the proposed method not only outperforms the other methods, it also shows practically acceptable level of performance.

Though the time taken by Mai [20], Bai [28], and Liu [44] is small, the superior performance of the proposed method as compared to them clearly outweighs the longer time taken by the proposed method. The proposed method is easily parallelizable and can give real time performance when optimized for specific applications.

Table 2. Performance metrics for the proposed method, Mai [20], Kim [21], Bai [28], Liu [44], and RHT [8] for real dataset (400 real images [26]).

	Proposed	Mai	Kim	Bai	Liu	RHT
Average Precision	0.8748	0.2862	0.1831	0.2248	0.0716	0.0213
Average Recall	0.7162	0.1632	0.1493	0.2955	0.1403	0.0157
Average F-measure	0.7548	0.1831	0.1591	0.1685	0.0808	0.0186
Average time taken (seconds)	38.68	11.41	60.87	9.10	7.78	810.41

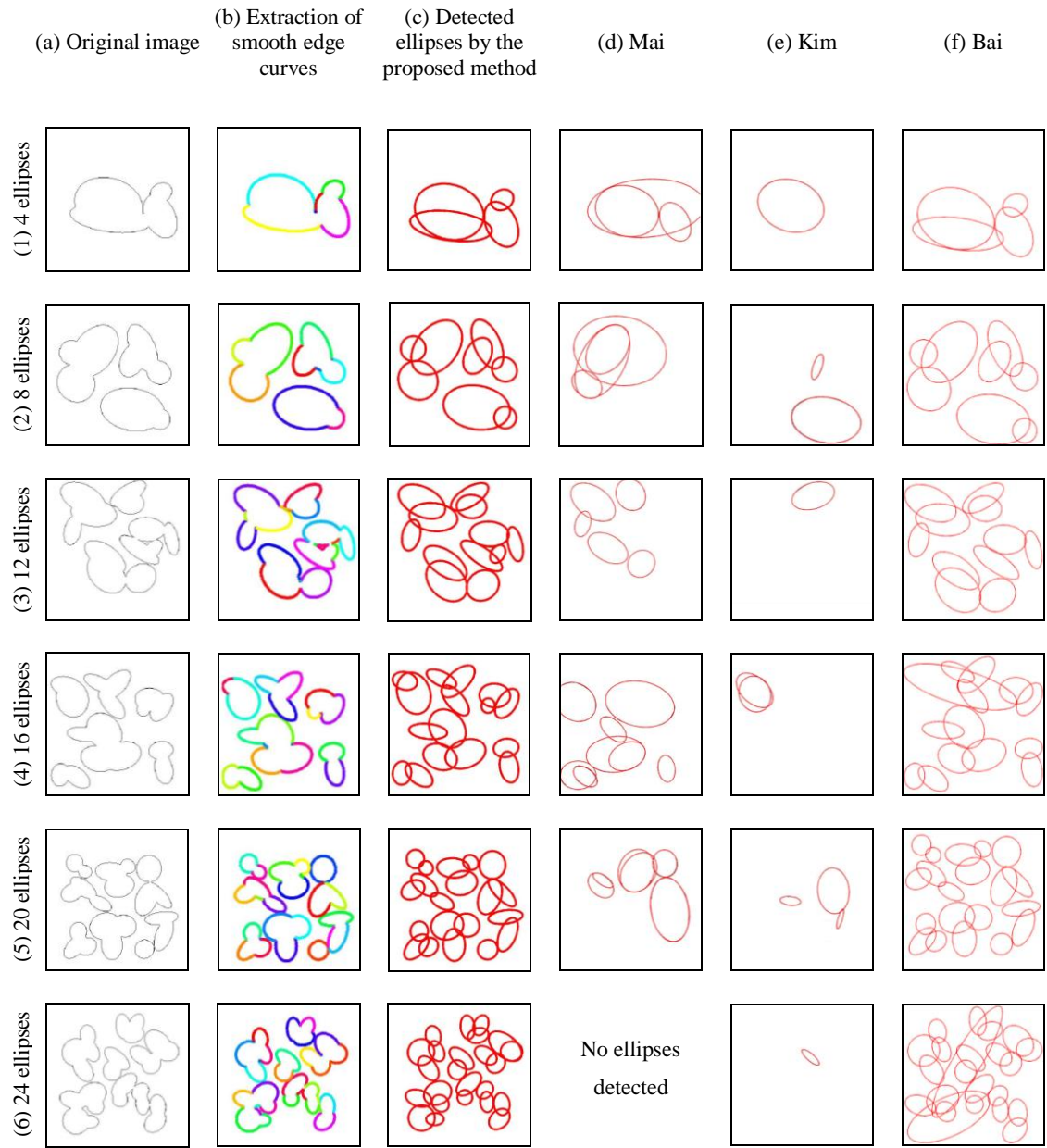


Fig. 15: Examples of synthetic images with occluded ellipses: proposed method vs. other methods.

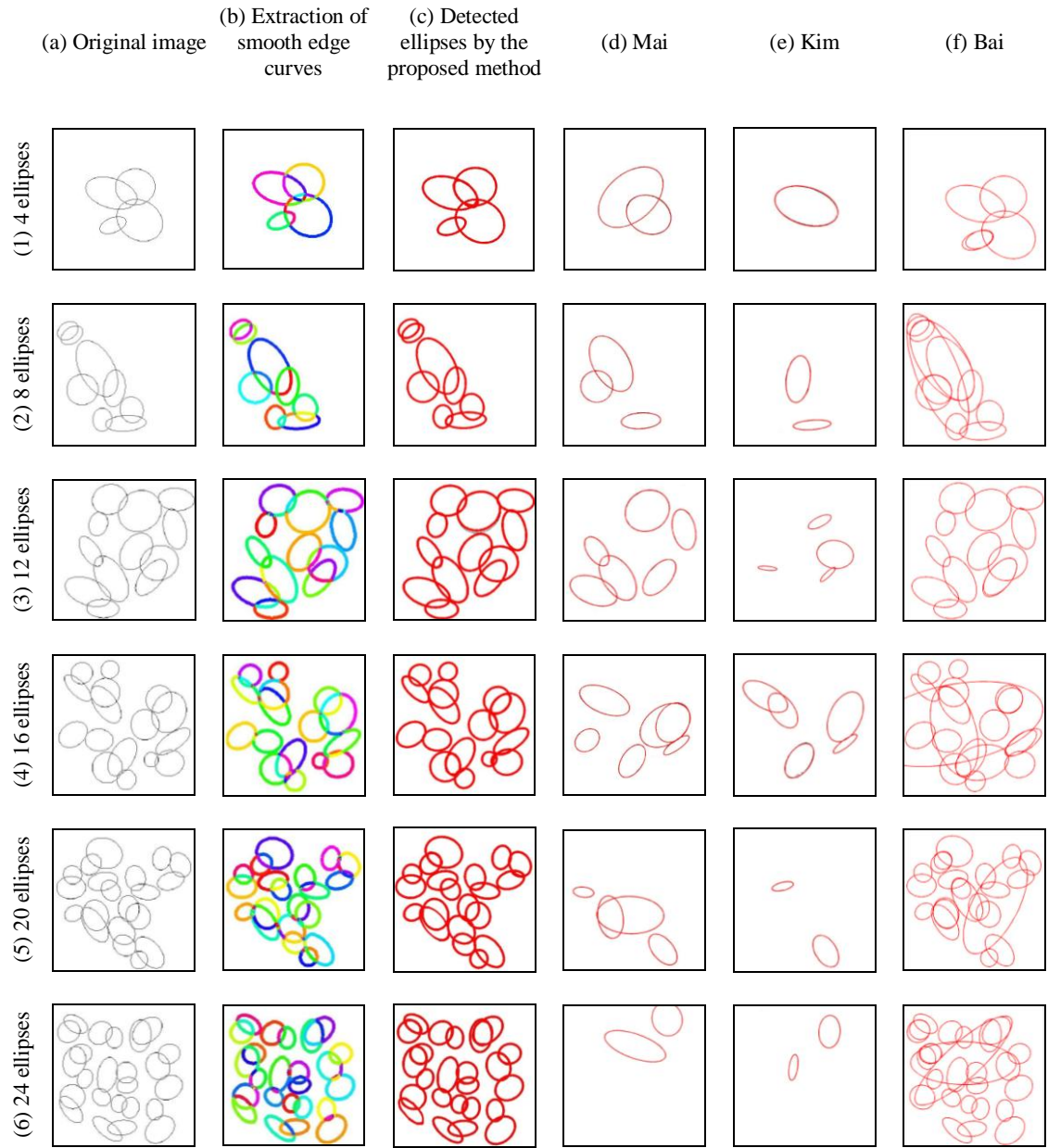


Fig. 16: Examples of synthetic images with overlapping ellipses: proposed method vs. other methods.

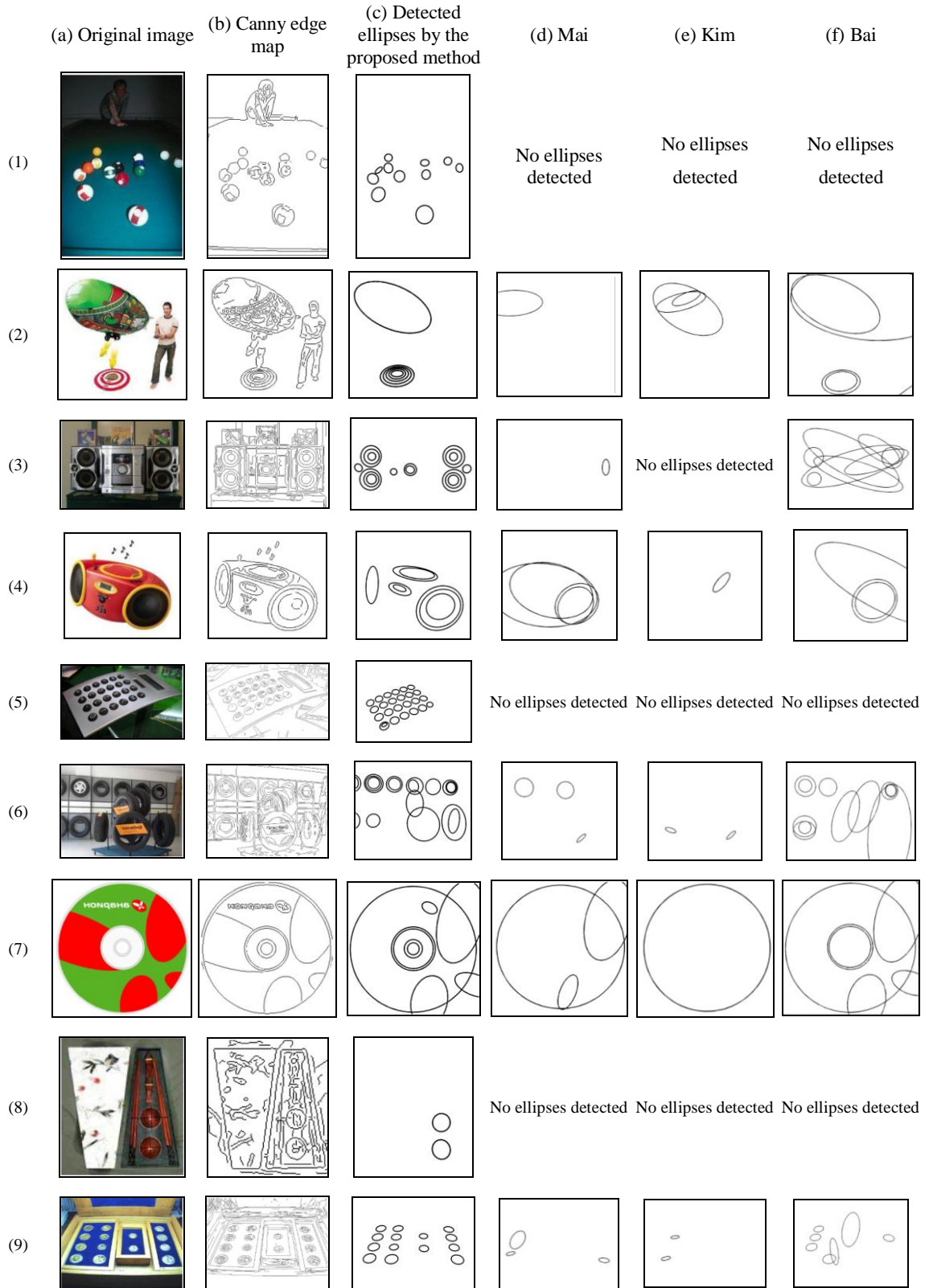


Fig. 17: Examples of real images: proposed method vs. other methods.

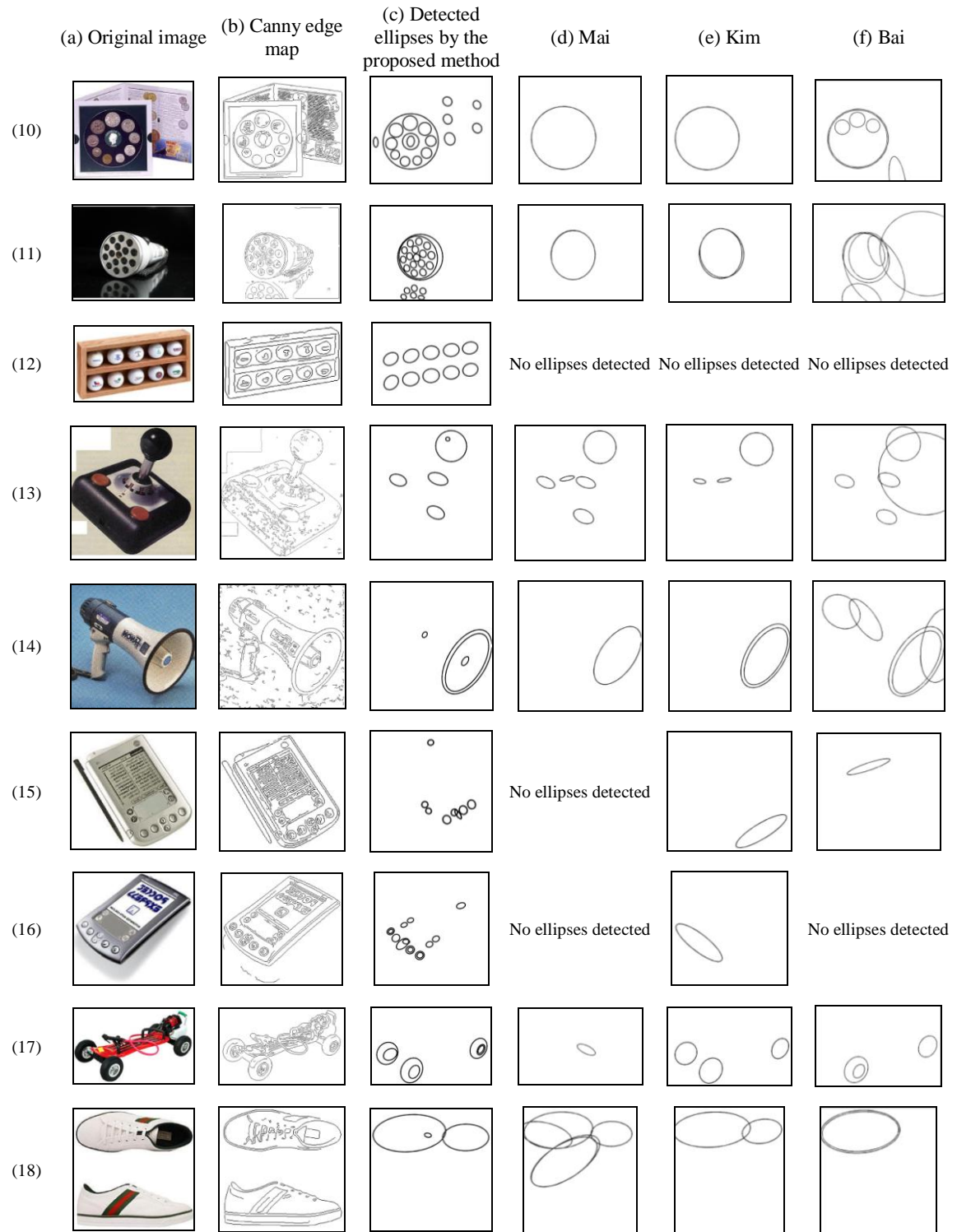


Fig. 17 (contd.): Examples of real images: proposed method vs. other methods.

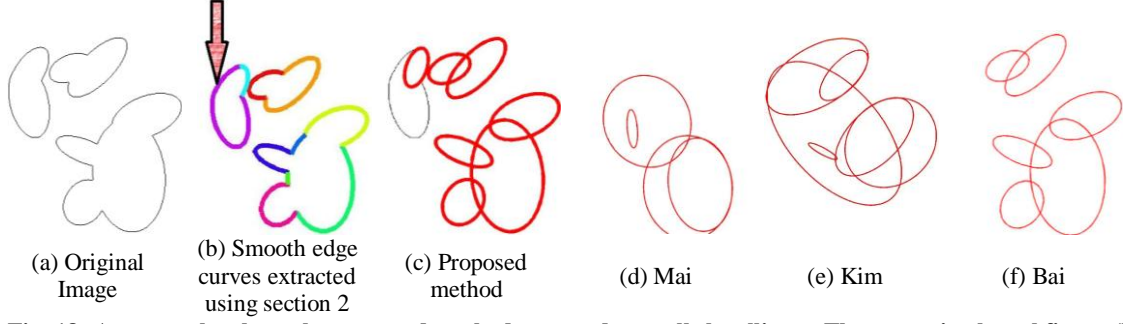


Fig. 18: An example where the proposed method cannot detect all the ellipses. The arrow in the subfigure (b) shows that the edge contours of two different ellipses were merged in such a manner that there is neither a sharp turn nor an inflexion point in region shown by the arrow. Due to this, the merged edge contour represents neither of the two ellipses.

Some detected examples of images with occluded and overlapping ellipses are presented in Fig. 15 and Fig. 16, respectively. We also present some examples of real images and the results of the proposed ellipse detection method in Fig. 17. For error analysis, we present an example of an image for which the proposed method cannot detect certain ellipses. Consider the example image shown in Fig. 18(a). The two left most ellipses have intersected each other in such a manner that there is no sharp turn or inflexion point at the left intersection point indicated by the arrow in Fig. 18(b). Due to this, the merged edge contour behaves as non-elliptic and does not get grouped with any other edge contours. Since the bigger left ellipse is represented only by this merged non-elliptic edge contour, this ellipse does not get detected in Fig. 18(c). The other methods are also unable to detect the ellipse (Fig. 18(d) – (f)).

5.5 A note on the influence of control parameters

We mention the control parameters and the influence of their choice on the performance of the proposed algorithm. For this purpose, we mention the control parameters and their individual effects below:

1. Edge contours less than 5 pixels long are omitted from consideration in the algorithm: They may be included as well. Including them does not have any effect on the performance of the algorithm except that the computation time increases significantly.

2. The threshold θ_0 for sharp turns detection (section 2.1): This is chosen heuristically and the performance of the algorithm does not significantly change in the range $\theta_0 \in [75^\circ, 105^\circ]$.

3. The control parameter R for tangent computation [39] used in section 3: The discussion about the choice of the control parameter is provided in [39]. Here, it suffices to mention that the performance of the method is not deteriorated for $R \in [3, 6]$. However, for very small ellipses (say semi-minor axis ~ 10), it is preferable to use $R = 3$ or 4 .

4. Size of the bins m, n and number of samples S used in section 3.4: An analysis of a suitable size of the bins is provided in [39, 41]. Here, we mention that $m, n \in [15, 50]$ generally do not deteriorate the performance of the method significantly. We note that a small bin size significantly increases the computation time while it is preferable to use more number of samples S if the bin size is increased. Our observation is that $S \approx 10 \min(m, n)$ is in general a good rule of thumb for an optimal tradeoff between the computation time and the number of groups.

5. Threshold parameter for least squares fitting ε_{ls} used in section 3.5: A suitable range of ε_{ls} is $[0.01, 0.1]$. However, for some very noisy images, it is preferable to choose ε_{ls} in the higher side of this range.

6. The allowable overlap ratio D_0 used in section 4.1: Generally usable values of D_0 are in the range $[0.8, 1]$. However, similar ellipses with very less difference are bound to occur in the proposed method and it is highly recommended that D_0 is chosen in the lower end of this range for good precision.

In summary, the proposed method has very few control parameters and the performance of the method is not very sensitive to the choice of control parameters in general. For every control parameter, the range of suitable values is large enough for a robust performance of the algorithm. In our opinion, this is one of the reasons for the superior performance of the proposed method in comparison with other methods.

6 Conclusion

This paper proposes a new method for ellipse detection, which performs significantly better than the existing methods for complicated synthetic and real images. The demonstrated performance is close to the best achievable performance for the synthetic images and high enough for real images to be used in practical applications. The primary reason of the good performance of the proposed method is the enhanced selectivity of the method while grouping the edge contours for detecting ellipses. The selectivity is due to the use of smooth curvature (in the form of search region and associated convexity), the novel relationship score, and the robust non-heuristic saliency criteria.

The performance of the ellipse detection method can be improved by use of better edge detectors that can enhance and selectively correct the edge contours where required. Further, better algorithms for extracting smooth edge curves that can deal with scenarios as shown in Fig. 18 shall also be helpful. Parallelization of the proposed method on the graphics processing units (GPU) shall enable real time application of the proposed method. These are the primary inspirations for the future work.

Other interesting future directions would include application of the proposed method for solving real life problems related to ellipse detection. The proposed method shows good performance for randomly chosen 400 real images from 48 categories of the Caltech 256 [26]. The Caltech 256 dataset is sufficiently complex and varied dataset with real images which emulate real life scenario sufficiently. Thus, the good performance of the proposed method indicates that the method can be widely used for practical applications. Some interesting application may be surface grain analysis of materials, medical diagnostics (like malarial/sickle cell counting), analysis of geological/astronomical pictures, assisted robotics for applications like sorting ores/ vegetables/ cans, etc. in automatic mineral processing/ grocery/ recycling units. For such dedicated applications, the method can be customized for better and faster performance. Advanced applications may include using the elliptic shapes for object detection [45], face detection [46], biometric iris based systems [47, 48], shape representation of complex objects [49], etc.

Acknowledgements

This work was supported in part by the Academic Research Fund Tier 1 (RG17/08 M52020088). We also thank Dr. F. Mai and Dr. R. A. McLaughlin for providing their executables and insights. We thank Dr. A. Y. S. Chia for his code on generating synthetic experimental data and his insights.

References

- [1] A. Fitzgibbon, M. Pilu, and R. B. Fisher, "Direct least square fitting of ellipses," *IEEE Transactions on Pattern Analysis and Machine Intelligence*, vol. 21 (5), pp. 476-480, 1999.
- [2] P. L. Rosin and G. A. W. West, "Nonparametric segmentation of curves into various representations," *IEEE Transactions on Pattern Analysis and Machine Intelligence*, vol. 17 (12), pp. 1140-1153, 1995.
- [3] P. L. Rosin, "Ellipse fitting by accumulating five-point fits," *Pattern Recognition Letters*, vol. 14 (8), pp. 661-669, 1993.
- [4] P. L. Rosin, "A note on the least squares fitting of ellipses," *Pattern Recognition Letters*, vol. 14 (10), pp. 799-808, 1993.
- [5] D. Chaudhuri, "A simple least squares method for fitting of ellipses and circles depends on border points of a two-tone image and their 3-D extensions," *Pattern Recognition Letters*, vol. 31 (9), pp. 818-829, 2010.
- [6] J. Cabrera and P. Meer, "Unbiased estimation of ellipses by bootstrapping," *IEEE Transactions on Pattern Analysis and Machine Intelligence*, vol. 18 (7), pp. 752-756, 1996.
- [7] R. O. Duda and P. E. Hart, *Pattern Classification and Scene Analysis*. New York: Wiley Publishers, 1973.
- [8] R. A. McLaughlin, "Randomized Hough transform: Improved ellipse detection with comparison," *Pattern Recognition Letters*, vol. 19 (3-4), pp. 299-305, 1998.
- [9] Z. G. Cheng and Y. C. Liu, "Efficient technique for ellipse detection using Restricted Randomized Hough Transform," in *Proceedings of the International Conference on Information Technology*, Las Vegas, NV, 2004, pp. 714-718.
- [10] N. Kiryati, Y. Eldar, and A. M. Bruckstein, "A probabilistic Hough transform," *Pattern Recognition*, vol. 24 (4), pp. 303-316, 1991.
- [11] N. Kiryati, H. Kalviainen, and S. Alaoutinen, "Randomized or probabilistic Hough transform: Unified performance evaluation," *Pattern Recognition Letters*, vol. 21 (13-14), pp. 1157-1164, 2000.

- [12] J. Illingworth and J. Kittler, "A survey of the hough transform," *Computer Vision, Graphics and Image Processing*, vol. 44 (1), pp. 87-116, 1988.
- [13] P. K. Ser and W. C. Siu, "Novel detection of conics using 2-D Hough planes," in *Proceedings of the IEE Vision, Image and Signal Processing*, 1995, pp. 262-270.
- [14] R. K. K. Yip, P. K. S. Tam, and D. N. K. Leung, "Modification of hough transform for circles and ellipses detection using a 2-dimensional array," *Pattern Recognition*, vol. 25 (9), pp. 1007-1022, 1992.
- [15] A. S. Aguado, M. E. Montiel, and M. S. Nixon, "On using directional information for parameter space decomposition in ellipse detection," *Pattern Recognition*, vol. 29 (3), pp. 369-381, 1996.
- [16] N. Guil and E. L. Zapata, "Lower order circle and ellipse Hough transform," *Pattern Recognition*, vol. 30 (10), pp. 1729-1744, 1997.
- [17] H. K. Yuen, J. Illingworth, and J. Kittler, "Detecting partially occluded ellipses using the Hough transform," *Image and Vision Computing*, vol. 7 (1), pp. 31-37, 1989.
- [18] H. X. Li, H. Zheng, and Y. Wang, "Segment Hough transform - a novel Hough-based algorithm for curve detection," in *Proceedings of the International Conference on Image and Graphics*, Chengdu, PEOPLES R CHINA, 2007, pp. 471-477.
- [19] T. Ellis, A. Abbood, and B. Brillault, "Ellipse detection and matching with uncertainty," *Image and Vision Computing*, vol. 10 (5), pp. 271-276, 1992.
- [20] F. Mai, Y. S. Hung, H. Zhong, and W. F. Sze, "A hierarchical approach for fast and robust ellipse extraction," *Pattern Recognition*, vol. 41 (8), pp. 2512-2524, 2008.
- [21] E. Kim, M. Haseyama, and H. Kitajima, "Fast and Robust Ellipse Extraction from Complicated Images," in *Proceedings of the International Conference on Information Technology and Applications*, 2002, pp. 357-362.
- [22] Y. Qiao and S. H. Ong, "Connectivity-based multiple-circle fitting," *Pattern Recognition*, vol. 37 (4), pp. 755-765, 2004.
- [23] Y. Qiao and S. H. Ong, "Arc-based evaluation and detection of ellipses," *Pattern Recognition*, vol. 40 (7), pp. 1990-2003, 2007.
- [24] Y. Xie and J. Ohya, "Elliptical object detection by a modified ransac with sampling constraint from boundary Curves' clustering," *IEICE Transactions on Information and Systems*, vol. E93-D (3), pp. 611-623, 2010.
- [25] A. Y. S. Chia, S. Rahardja, D. Rajan, and M. K. Leung, "A Split and Merge Based Ellipse Detector With Self-Correcting Capability," *Image Processing, IEEE Transactions on*, vol. 20 (7), pp. 1991-2006, 2011.
- [26] G. Griffin, A. Holub, and P. Perona. *Caltech-256 object category database* [<http://authors.library.caltech.edu/7694>]. Available: <http://authors.library.caltech.edu/7694>
- [27] Y. Chi and M. K. H. Leung, "Part-based object retrieval in cluttered environment," *IEEE Transactions on Pattern Analysis and Machine Intelligence*, vol. 29 (5), pp. 890-895, 2007.
- [28] X. Bai, C. Sun, and F. Zhou, "Splitting touching cells based on concave points and ellipse fitting," *Pattern Recognition*, vol. 42 (11), pp. 2434-2446, 2009.
- [29] S. C. Zhang and Z. Q. Liu, "A robust, real-time ellipse detector," *Pattern Recognition*, vol. 38 (2), pp. 273-287, 2005.
- [30] Y. C. Cheng, "The distinctiveness of a curve in a parameterized neighborhood: Extraction and applications," *IEEE Transactions on Pattern Analysis and Machine Intelligence*, vol. 28 (8), pp. 1215-1222, 2006.
- [31] C. A. Basca, M. Talos, and R. Brad, "Randomized hough transform for ellipse detection with result clustering," in *Proceedings of the International Conference on Computer as a Tool*, Belgrade, SERBIA MONTENEG, 2005, pp. 1397-1400.
- [32] J. Princen, J. Illingworth, and J. Kittler, "Hypothesis testing - a framework for analyzing and optimizing Hough transform performance," *IEEE Transactions on Pattern Analysis and Machine Intelligence*, vol. 16 (4), pp. 329-341, 1994.

- [33] [C. Wang, T. S. Newman, and C. Cao, "New hypothesis distinctiveness measure for better ellipse extraction," in *Lecture Notes in Computer Science* vol. 4633, ed, 2007, pp. 176-186.](#)
- [34] R. C. Gonzalez and R. E. Woods, *Digital Image Processing*, 3 ed. Delhi: Pearson Prentice Hall, 2008.
- [35] P. D. Kovesi. *MATLAB and Octave Functions for Computer Vision and Image Processing* (2000 ed.) [<http://www.csse.uwa.edu.au/~pk/Research/MatlabFns/index.html>].
- [36] [D. K. Prasad, M. K. H. Leung, S. Y. Cho, and C. Quek, "A parameter independent line fitting method," in *Asian Conference on Pattern Recognition \(ACPR\)*, Beijing, China, 2011, pp. 441-445.](#)
- [37] U. Ramer, "An iterative procedure for the polygonal approximation of plane curves," *Computer Graphics and Image Processing*, vol. 1 (3), pp. 244-256, 1972.
- [38] D. H. Douglas and T. K. Peucker, "Algorithms for the reduction of the number of points required to represent a digitized line or its caricature," *Cartographica: The International Journal for Geographic Information and Geovisualization*, vol. 10 (2), pp. 112-122, 1973.
- [39] D. K. Prasad, R. K. Gupta, and M. K. H. Leung, "An Error Bounded Tangent Estimator for Digitized Elliptic Curves," in *Lecture Notes in Computer Science*. vol. 6607, ed: Springer Berlin / Heidelberg, 2011, pp. 272-283.
- [40] F. De Vieilleville and J. O. Lachaud, "Comparison and improvement of tangent estimators on digital curves," *Pattern Recognition*, vol. 42 (8), pp. 1693-1707, 2009.
- [41] D. K. Prasad and M. K. H. Leung, "Error analysis of geometric ellipse detection methods due to quantization," in *Fourth Pacific-Rim Symposium on Image and Video Technology (PSIVT 2010)*, Singapore, 2010, pp. 58 - 63.
- [42] P. N. Tan, M. Steinbach, and V. Kumar, *Introduction to Data Mining*: Pearson Addison Wesley, 2006.
- [43] [D. K. Prasad and M. K. H. Leung, "An ellipse detection method for real images," in *25th International Conference of Image and Vision Computing New Zealand \(IVCNZ 2010\)*, Queenstown, New Zealand, 2010, pp. 1-8.](#)
- [44] [Z. Y. Liu and H. Qiao, "Multiple ellipses detection in noisy environments: A hierarchical approach," *Pattern Recognition*, vol. 42 \(11\), pp. 2421-2433, 2009.](#)
- [45] [A. Y. S. Chia, S. Rahardja, D. Rajan, and M. K. H. Leung, "Structural descriptors for category level object detection," *IEEE Transactions on Multimedia*, vol. 11 \(8\), pp. 1407-1421, 2009.](#)
- [46] [H. S. Kim, W. S. Kang, J. I. Shin, and S. H. Park, "Face detection using template matching and ellipse fitting," *IEICE Transactions on Information and Systems*, vol. E83-D \(11\), pp. 2008-2011, 2000.](#)
- [47] [X. Feng, C. Fang, X. Ding, and Y. Wu, "Iris localization with dual coarse-to-fine strategy," in *Proceedings of the International Conference on Pattern Recognition*, 2006, pp. 553-556.](#)
- [48] [X. He and P. Shi, "A novel Iris segmentation method for hand-held capture device," in *Lecture Notes in Computer Science* vol. 3832, ed, 2006, pp. 479-485.](#)
- [49] [P. F. Felzenszwalb and D. P. Huttenlocher, "Pictorial structures for object recognition," *International Journal of Computer Vision*, vol. 61 \(1\), pp. 55-79, 2005.](#)